# Saddle-splay-term-induced orientational instability in nematic-liquid-crystal cells and director fluctuations at substrates

A. D. Kiselev*
*Chernigov State Technological University, Shevchenko Street 95, 14027 Chernigov, Ukraine*
(Received 13 September 2003; revised manuscript received 13 November 2003; published 14 April 2004)

We analyze stability of the planar orientational structure in a nematic-liquid-crystal cell with planar anchoring conditions at both substrates. Specifically, we study the instabilities of the ground state caused by surface elasticity with the saddle-splay elastic constant $K_{24}$ violating the Ericksen inequalities. We express the surface part of static correlation functions as a functional integral over the fluctuation field induced by director fluctuations at confining walls and derive the stability conditions for the planar structure with respect to the fluctuation modes characterized by the in-plane wave numbers and by the parity. These conditions are analyzed in the cell thickness–fluctuation wavelength plane through the parametrization for the boundary curve of the instability region. For relatively small $K_{24}$, the fluctuation mode of the critical wavelength is found to render the structure unstable when the thickness of the cell is below its critical value. The parity of the critical mode changes as the twist-splay ratio $K_2/K_1$ is passing through unity. Further increase of $K_{24}$ beyond the second threshold value, $4K_1K_2/(K_1+K_2)$, leads to the instability with respect to short wavelength fluctuations regardless of the cell thickness. We compute the critical thickness and the critical wavelength as a function of $K_{24}$, the twist-splay ratio, and the azimuthal anchoring strength.

DOI: 10.1103/PhysRevE.69.041701 PACS number(s): 61.30.Gd, 64.70.Md, 61.30.Hn

## I. INTRODUCTION

Nematic liquid crystals (NLCs) confined in restricted geometries are technologically important [1] and have been the subject of intense studies over the past few decades [2,3]. Anisotropy of the vast majority of NLCs is locally uniaxial and molecules of a NLC align on average along a local unit director. Orientational structures in NLCs are thus defined by distributions of the director $\mathbf{n}(\mathbf{r})$ and the well-established continuum elastic theory provides the phenomenological description of orientational distortions [4,5].

In the absence of external fields, orientational structures in spatially bounded NLCs crucially depend on the conditions at confining walls. These are macroscopically characterized by the surface contribution to the elastic free energy $F_s$ that adds to the Frank elastic energy $F_b$, describing elasticity of NLC in the bulk, to yield the total elastic free energy of a NLC in the presence of the confining surfaces:

$$F[\mathbf{n}]=F_b[\mathbf{n}]+F_s[\mathbf{n}], \tag{1}$$

$$F_b=\frac{1}{2}\int_V\{K_1(\boldsymbol{\nabla},\mathbf{n})^2+K_2(\mathbf{n},\boldsymbol{\nabla}\times\mathbf{n})^2+K_3[\mathbf{n}\times(\boldsymbol{\nabla}\times\mathbf{n})]^2\}dv, \tag{2}$$

$$F_s=\frac{1}{2}\int_S\{W(\mathbf{n})-K_{24}[(\boldsymbol{\nu},\mathbf{n})(\boldsymbol{\nabla},\mathbf{n})-(\boldsymbol{\nu},(\mathbf{n},\boldsymbol{\nabla})\mathbf{n})]\}ds, \tag{3}$$

where $K_1$, $K_2$, and $K_3$ are the splay, twist, and bend elastic constants, respectively, $K_{24}$ is the saddle-splay elastic constant, $\boldsymbol{\nu}$ is the outer normal to the surface $S$, and $W(\mathbf{n})$ is the surface density of the anchoring energy.

An important point is that, in addition to the anchoring energy which is the anisotropic part of the surface tension, there is also the elastic contribution to the surface free energy that, originally, has been indicated as a part of the elastic energy having the form of a divergence [6–8]. This contribution—the so-called saddle-splay term (the $K_{24}$ term)—can generally be viewed as the tangential director gradient dependent elastic part of the surface energy [9,10]. The other surface elastic term known as the $K_{13}$ term will not be considered in this paper as it can be ignored in cases where spatial variations of the density and the scalar order parameter are of minor importance [11–13].

In the last years $K_{24}$ specific issues have attracted much less attention than the fundamental difficulties caused by the $K_{13}$ term. In particular, though the exact measurements of $K_{24}$ are still missing it was experimentally estimated to be of the order of the Frank elastic constants [14–16]. One of the most important theoretical results is that the $K_{24}$ term may induce spontaneous twist deformations in hybrid nematic films with azimuthally degenerate anchoring conditions [17]. Such deformations are manifested in the formation of periodic stripe domains observed in sufficiently thin hybrid NLC cells [18–20].

For planar NLC cells, similar instability of the ground state in the presence of the $K_{24}$ term was considered in Refs. [21,22]. Recently, in Ref. [23], Barbero and Pergamenshchik suggested that in the proximity of the nematic-smectic-*A* transition the $K_{24}$ term grows anomalously large so as to violate the Ericksen stability conditions [24]:

$$0<K_{24}<2\ \min(K_1,K_2). \tag{4}$$

As a result, the uniform equilibrium director distribution be-

*Email address: kisel@mail.cn.ua

 

comes unstable and a periodically modulated nematic phase may occur in sufficiently thin planar films.

The results of Refs. [22,23,25] are essentially limited to the special case in which the azimuthal anchoring strength is identically zero. But the study of possible mechanisms leading to the formation of modulated orientational structures close to the nematic-smectic-*A* transition requires a quantitatively accurate description of the instability that goes beyond this limitation. At this stage, however, even the instability scenario as a whole has not been studied in any detail.

In this paper we intend to fill the gap. Our primary goal is the comprehensive study of the instability induced by the $K_{24}$ term in the presence of the azimuthal anchoring.

The idea underlying our general theoretical considerations is that instabilities of this sort occur when the director fluctuations at confining surfaces become critically divergent. So, we suggest the method connecting the correlation functions of director fluctuations and the computational procedure applied to perform the stability analysis. This method is based on separating out the surface part of the correlator as a correlation function of the fluctuation field induced by the director fluctuations at confining walls.

The layout of the paper is as follows. In Sec. II, we express the surface part of the static correlation functions of the director fluctuations as a functional integral over fluctuations at confining walls and explicitly relate the procedure for computing the correlators to the stability conditions used in our stability analysis.

Analytical results for the planar NLC cell are described in Sec. III. We characterize the mirror symmetry properties of the fluctuation harmonics and calculate the surface part of the correlator. We find that the result is a sum of the contributions from the two fluctuation modes of different symmetry (symmetric and antisymmetric) and derive the stability conditions for these modes.

Stability of the uniform planar orientational structure is studied in Sec. IV. We analyze the parametrization of the boundary curve enclosing the instability region in the thickness-wavelength plane and show that, in addition to the stability interval (4), there are two different intervals for $K_{24}$: (a) $2\min(K_1,K_2)<K_{24}<4K_1K_2/(K_1+K_2)$, where the critical point is characterized by the critical thickness $d_c$ and the critical fluctuation wavelength $\lambda_c$; (b) $K_{24}>4K_1K_2/(K_1+K_2)$, where NLC cells of any thickness are unstable with respect to the short wavelength fluctuations with $\lambda<\lambda_\infty$. It is found that the critical fluctuation mode is antisymmetric at $K_2<K_1$ and is symmetric at $K_2>K_1$. The critical thickness and the critical wavelength are computed as functions of $K_{24}$ and the azimuthal anchoring strength. We also discuss the spectrum of director fluctuations at the substrates near the critical thickness.

Finally, in Sec. V, we present our results and make some concluding remarks.

## II. CORRELATION FUNCTIONS AND STABILITY CRITERIA

In this section we consider the general procedure for computing the correlation functions (correlators) of NLC director fluctuations in confined liquid crystals. After introducing necessary notations we briefly remind the reader about the standard approach that uses functional integrals to carry out averaging over fluctuations [5,26]. In this approach the effect of the confining surface enters the theory through the boundary conditions for the saddle point equations (Euler-Lagrange equations) and for the Green functions.

We then describe an alternative procedure, where the part of the fluctuation field representing the director fluctuations at the surface is separated out by shifting the integration variable in the functional integral. The corresponding part of the correlator is defined by the surface part of the free energy (3) and involves averaging over the fluctuations at the surface. Finally, we show that the energy of these fluctuations determines stability of orientational structures. Some technical details omitted in this paper can be found in Ref. [27].

### A. Energy of director distortions and static correlation functions

Assuming that the director field $\mathbf{n}_0$ defines the unperturbed orientational structure, we begin with the distorted director configuration

$$\mathbf{n}=\cos\theta\cos\phi\,\mathbf{n}_0+\cos\theta\sin\phi\,\mathbf{n}_1+\sin\theta\,\mathbf{n}_2,$$

$$(\mathbf{n}_i,\mathbf{n}_j)=\delta_{ij}, \tag{5}$$

where brackets denote the scalar product. For small distortions with $\phi,\theta\ll 1$, Eq. (5) reduces to the familiar form

$$\mathbf{n}\approx\mathbf{n}_0+\delta\mathbf{n}_0,\quad \delta\mathbf{n}_0=\psi_i\,\mathbf{n}_i, \tag{6}$$

where the angles $\phi$ and $\theta$ representing fluctuations of the director are conveniently combined into the two-component fluctuation field: $\boldsymbol{\psi}\equiv\binom{\psi_1}{\psi_2}=\binom{\phi}{\theta}$ and summation over repeated indices will be assumed throughout the paper.

The elastic energy of the fluctuation field $\boldsymbol{\psi}$ can be derived from the free energy of the director configuration (5) obtained by substituting Eq. (5) into Eqs. (1)–(3). In the lowest order approximation—the so-called Gaussian approximation—this energy is given by the second-order term $F^{(2)}$ of the truncated series expansion for the free energy functional (1),

$$F[\mathbf{n}]\approx F[\mathbf{n}_0]+F^{(2)}[\boldsymbol{\psi}], \tag{7}$$

$$F^{(2)}[\boldsymbol{\psi}]=F_b^{(2)}[\boldsymbol{\psi}]+F_s^{(2)}[\boldsymbol{\psi}], \tag{8}$$

where $F_b^{(2)}$ and $F_s^{(2)}$ are the bulk and the surface parts of the fluctuation energy generated by the corresponding terms of the free energy (1).

The standard variational procedure provides the saddle point equations for $F^{(2)}[\boldsymbol{\psi}]$ in the following general form:

$$\frac{\delta F_b^{(2)}[\boldsymbol{\psi}]}{\delta\psi_i(\mathbf{r})}=\hat{K}_{ij}\psi_j(\mathbf{r})\equiv\hat{K}\boldsymbol{\psi}(\mathbf{r})=0, \tag{9}$$

where $\hat{K}$ is the matrix differential operator and hats indicate matrices and matrix differential operators. These equations can also be derived as the linearized Euler-Lagrange equations for the director (5).

The general structure of the fluctuation energy (8) can now be expressed as follows:

$$F_b^{(2)}[\boldsymbol{\psi}] = \int_V (\boldsymbol{\psi}, \hat{K}\boldsymbol{\psi})\, dv + \int_S (\boldsymbol{\psi}, \hat{Q}^{(b)}\boldsymbol{\psi})\, ds, \tag{10}$$

$$F_s^{(2)}[\boldsymbol{\psi}] = \int_S (\boldsymbol{\psi}, \hat{Q}^{(s)}\boldsymbol{\psi})\, ds. \tag{11}$$

where $(\boldsymbol{\varphi}, \hat{A}\boldsymbol{\psi}) \equiv \varphi_i \hat{A}_{ij} \psi_j$ and the last surface term on the right-hand side of Eq. (10) results from the integration by parts.

We shall need to write the probability distribution of fluctuations at the state of thermal equilibrium in the form

$$P[\boldsymbol{\psi}] = Z^{-1} \exp\{-\beta F^{(2)}[\boldsymbol{\psi}]\}, \tag{12}$$

where $\beta \equiv (k_B T)^{-1}$, $k_B$ is the Boltzmann constant, $T$ is the temperature, and $Z$ is the partition function given by the functional integral

$$Z = \int \exp\{-\beta F^{(2)}[\boldsymbol{\psi}]\} \mathcal{D}\boldsymbol{\psi}, \tag{13}$$

where $\mathcal{D}\boldsymbol{\psi} \equiv \mathcal{D}\psi_1 \mathcal{D}\psi_2$. The averages of the fluctuation field products

$$C_{ij}(\mathbf{r}, \mathbf{r}') \equiv [\hat{C}(\mathbf{r}, \mathbf{r}')]_{ij} = \langle \psi_i(\mathbf{r}) \psi_j(\mathbf{r}') \rangle = \int \psi_i(\mathbf{r}) \psi_j(\mathbf{r}') P[\boldsymbol{\psi}] \mathcal{D}\boldsymbol{\psi} \tag{14}$$

then give the components of the correlator which is more appropriately known as the two-point static correlation function [26].

Explicit analytical treatment of functional integrals can be rather involved [28]. One way around the difficulties is to introduce the generating functional of the correlation functions through the partition function of the distribution (12) with the energy (8) augmented by a source term [26].

Following Ref. [27], the standard relations linking the correlator and functional derivatives of the generating functional can be used to show that the correlator is proportional to the Green function of the operator $\hat{K}$,

$$\hat{C}(\mathbf{r}, \mathbf{r}') = \beta^{-1} \hat{G}(\mathbf{r}, \mathbf{r}'), \tag{15}$$

and the boundary value problem for the Green function $\hat{G}$ is

$$\hat{K}_{ik} G_{kj}(\mathbf{r}, \mathbf{r}') = \delta(\mathbf{r} - \mathbf{r}')\, \delta_{ij}, \tag{16a}$$

$$\hat{Q}_{ik} G_{kj}(\mathbf{r}, \mathbf{r}')\big|_{\mathbf{r} \in S} = 0, \tag{16b}$$

where $\hat{Q} = \hat{Q}^{(b)} + \hat{Q}^{(s)}$ and $\delta(\mathbf{r})$ is the delta function.

The problem (16) is at the heart of the conventional computational procedures traditionally used, e.g., in studies of light scattering in confined liquid crystals [29–33].

The key point is that the effects caused by the anchoring energy and the surface elasticity constant are solely incorporated into the boundary conditions (16b). These conditions affect eigenfunctions (normal fluctuation modes) and eigenvalues of the operator $\hat{K}$. The eigenvalues form the spectrum of fluctuations that must be positive provided the orientational structure $\mathbf{n}_0$ is stable. Otherwise, the functional integrals (13) and (14) do not converge.

We have thus formulated the spectral stability conditions that turn out to be closely related to the approach based on the generating functional. These conditions are in considerable use as stability criteria in several methods developed to study Fréedericksz-type transitions in confined liquid crystals [34,35].

### B. Surface part of correlator and stability

We now pass on to the approach that emphasizes the role of the director fluctuations at confining walls by using another transformation of the functional integral (14). This transformation has long been known as an efficient method to perform Gaussian integrals [26] and we, following the general idea, define the new integration variable $\boldsymbol{\varphi}_b$ that vanishes at the surface by translating the fluctuation field $\boldsymbol{\psi}$:

$$\boldsymbol{\psi} = \boldsymbol{\varphi}_b + \boldsymbol{\varphi}, \quad \boldsymbol{\varphi}_b\big|_S = 0, \tag{17}$$

where $\boldsymbol{\varphi}_b = \begin{pmatrix} \varphi_1^{(b)} \\ \varphi_2^{(b)} \end{pmatrix}$.

The fluctuation field $\boldsymbol{\psi}$ is thus decomposed into the field $\boldsymbol{\varphi}_b$ vanishing at the surface and the field $\boldsymbol{\varphi}$ that accounts for nonvanishing fluctuations at the surface, $\boldsymbol{\psi}|_S = \boldsymbol{\varphi}_s$. When $\boldsymbol{\varphi}$ additionally satisfies the Euler-Lagrange equations (9),

$$\hat{K}\boldsymbol{\varphi} = 0, \quad \boldsymbol{\varphi}\big|_S = \boldsymbol{\psi}\big|_S \equiv \boldsymbol{\varphi}_s, \tag{18}$$

the fluctuations described by $\boldsymbol{\varphi}_b$ and $\boldsymbol{\varphi}$ will be statistically independent [27],

$$F^{(2)}[\boldsymbol{\varphi}_b + \boldsymbol{\varphi}] = F_b^{(2)}[\boldsymbol{\varphi}_b] + \Phi_s[\boldsymbol{\varphi}_s], \tag{19}$$

$$\Phi[\boldsymbol{\varphi}_s] = \int_S (\boldsymbol{\varphi}_s, \hat{Q}\boldsymbol{\varphi}_s)\, ds \tag{20}$$

and combining Eqs. (19) and (12) gives the probability distributions

$$P_b[\boldsymbol{\varphi}_b] = Z_b^{-1} \exp\{-\beta F_b^{(2)}[\boldsymbol{\varphi}_b]\}, \tag{21}$$

$$P_s[\boldsymbol{\varphi}_s] = Z_s^{-1} \exp\{-\beta \Phi_s[\boldsymbol{\varphi}_s]\}, \tag{22}$$

where $P_b[\boldsymbol{\varphi}_b]$ is the distribution for the field of fluctuations in the bulk $\boldsymbol{\varphi}_b$, and the distribution $P_s[\boldsymbol{\varphi}_s]$ characterizes the fluctuations at the surface $\boldsymbol{\varphi}_s$.

Averaging over the fluctuation fields $\boldsymbol{\varphi}_s$ and $\boldsymbol{\varphi}_b$ can now be performed independently. As a result, we have

$$\langle A_b A_s \rangle = \int A_b A_s P[\boldsymbol{\psi}] \mathcal{D}\boldsymbol{\psi}$$

$$= \int A_s P_s[\boldsymbol{\varphi}_s] \mathcal{D}\boldsymbol{\varphi}_s \int_{\boldsymbol{\varphi}_b|_S = 0} A_b P_b[\boldsymbol{\varphi}_b] \mathcal{D}\boldsymbol{\varphi}_b$$

$$= \langle A_s \rangle_s \langle A_b \rangle_b , \tag{23}$$

where $A_s \equiv A_s[\boldsymbol{\varphi}_s]$ and $A_b \equiv A_b[\boldsymbol{\varphi}_b]$.

After substituting the decomposition (17) into Eq. (14) and using Eq. (23) to carry out averaging over fluctuations we arrive at the expression for the correlator in the final form

$$C_{ij}(\mathbf{r},\mathbf{r}') = C_{ij}^{(b)}(\mathbf{r},\mathbf{r}') + C_{ij}^{(s)}(\mathbf{r},\mathbf{r}'). \tag{24}$$

The two terms on the right-hand side of Eq. (24) are given by

$$C_{ij}^{(b)}(\mathbf{r},\mathbf{r}') = \langle \varphi_i^{(b)}(\mathbf{r}) \varphi_j^{(b)}(\mathbf{r}') \rangle_b , \tag{25}$$

$$C_{ij}^{(s)}(\mathbf{r},\mathbf{r}') = \langle \varphi_i(\mathbf{r}|\boldsymbol{\varphi}_s) \varphi_j(\mathbf{r}'|\boldsymbol{\varphi}_s) \rangle_s , \tag{26}$$

where notations for the argument of $\boldsymbol{\varphi}$ indicate the dependence of the field $\boldsymbol{\varphi}$ on $\boldsymbol{\varphi}_s$ [see Eq. (18)].

The correlator $\hat{C}^{(b)}$ is entirely determined by the bulk director fluctuations with the probability distribution (21). In this case the fluctuations at the surface are suppressed and the boundary conditions for $\hat{C}^{(b)}$,

$$C_{ij}^{(b)}(\mathbf{r},\mathbf{r}')|_{\mathbf{r}\in S} = 0, \tag{27}$$

correspond to the limit of infinitely strong anchoring for Eq. (16b).

When the anchoring is not infinitely strong, the boundary conditions (16b) differ from the strong anchoring conditions (27). Now the fluctuations at the confining wall have not been suppressed completely and are characterized by the probability distribution (22) with the energy (20). Equation (18) shows that these fluctuations transmitted into the bulk give rise to the fluctuation field $\boldsymbol{\varphi}$. Equation (26) gives the correlator of the field $\boldsymbol{\varphi}$ induced by the fluctuations at the surface and determines the difference between $\hat{C}$ and $\hat{C}^{(b)}$. In what follows the correlator $\hat{C}^{(s)}$ will be referred to as the surface part of the correlator $\hat{C}$.

It is of particular interest that the surface part of the correlator is written as an average with the distribution (22). When the energy (20) is not positive definite and the conditions

$$(\boldsymbol{\varphi}_s, \hat{Q}\boldsymbol{\varphi}_s) > 0 \tag{28}$$

are violated, the correlator (26) becomes divergent. So, stability of the orientational structure with respect to the director fluctuations at the confining surface is determined by the stability conditions (28). Instabilities induced by such fluctuations are of our primary concern, since neither the anchoring energy nor the $K_{24}$ term may affect the correlator of the bulk fluctuation field (25).

Technically, using the conditions (28) enormously simplifies stability analysis as compared to exploring the spectrum of fluctuations [35]. The procedure involves two steps: (a) solving the boundary value problem for the Euler-Lagrange equations (18), and (b) evaluating the energy of the fluctuations at the surface (20). Finally, the stability conditions are derived as the conditions for the energy to be positive definite.

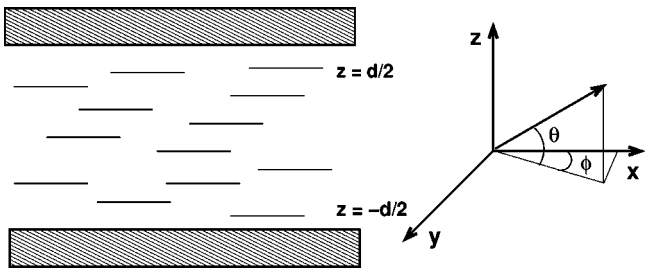


FIG. 1. Schematic representation of the planar NLC cell. The angles $\phi$ and $\theta$ describe the in-plane and the out-of-plane director fluctuations, respectively.

Equivalent computational schemes have already been used to study surface elasticity effects in Refs. [21,25,36]. We have thus developed the method at the very least linking these schemes and the surface part of the correlator that takes into account the director fluctuations at the confining surface.

In the following section we apply the above described procedure to the case of the planar orientational structure in a NLC cell. As an advantage of our approach, the study of director fluctuations at the substrates bounding the cell will be naturally incorporated into the stability analysis.

## III. DIRECTOR FLUCTUATIONS IN NEMATIC CELL

In this section we consider a NLC planar cell of the thickness $d$ sandwiched between two substrates that are both normal to the $z$ axis: $z = -d/2$ and $z = d/2$. Anchoring conditions at both substrates are planar with the vector of easy orientation directed along the $x$ axis. Thus, we have the uniform planar director distribution $\mathbf{n}_0 = \mathbf{e}_x$ giving the ground state undistorted orientational structure.

The distorted director (5) with $\mathbf{n}_1 = \mathbf{e}_y$ and $\mathbf{n}_2 = \mathbf{e}_z$ is characterized by the angles $\phi$ and $\theta$ shown in Fig. 1. For small angles, the approximate second-order expression for the anchoring potential is

$$W(\mathbf{n}) \approx W(\mathbf{n}_0) + W_\theta \theta^2 + W_\phi \phi^2, \tag{29}$$

where $W_\theta$ and $W_\phi$ are the zenithal and the azimuthal anchoring strengths. Note that Eq. (29) does not imply using the Rapini-Papoular potential [37], where $W_\theta = W_\phi$. But the surface energy costs for splay-bend and twist director deformations in interfacial layers are generally different (recent discussion can be found in Ref. [38]). So, it is more reasonable to consider the case in which the zenithal and the azimuthal anchoring energies differ.

The cell is invariant under translations in the $x$-$y$ plane and we impose the periodic conditions on the fluctuation field: $\boldsymbol{\psi}(x+L_x, y, z) = \boldsymbol{\psi}(x, y, z)$ and $\boldsymbol{\psi}(x, y+L_y, z) = \boldsymbol{\psi}(x, y, z)$, where $L_x$ and $L_y$ are the characteristic lengths of the

cell along the $x$ and $y$ axes, respectively. We can now write down the Fourier series expansion for the fluctuations:

$$\boldsymbol{\psi}=\sum_{\mathbf{m},m_y\geqslant 0}\{\boldsymbol{\psi}_{\mathbf{m}}(z)\exp[i(k_x x+k_y y)] + \boldsymbol{\psi}^{*}_{\mathbf{m}}(z)\exp[-i(k_x x+k_y y)]\}, \tag{30}$$

where $\mathbf{m}=(m_x,m_y)$, $k_x=2\pi m_x/L_x$, $k_y=2\pi m_y/L_y$ and an asterisk indicates complex conjugation.

Since the fluctuation harmonics with nonvanishing $k_x$ do not produce additional instability, we shall restrict ourselves to the case in which $k_x=0$. Owing to the translational symmetry, the fluctuation harmonics are statistically independent in the Gaussian approximation and the energy of fluctuations takes the form of a sum of the energies of different fluctuation modes:

$$F^{(2)}[\boldsymbol{\psi}]=\sum_{m\geqslant 0}(2-\delta_{m,0})F^{(2)}_{m}[\boldsymbol{\psi}_m], \tag{31}$$

where $m\equiv m_y$.

Calculation of the fluctuation energy is rather straightforward [27] and we present the result in matrix notations for the modified fluctuation harmonics:

$$\boldsymbol{\psi}_m\rightarrow\boldsymbol{\psi}=\begin{pmatrix}1 & 0\\ 0 & i\end{pmatrix}\boldsymbol{\psi}_m. \tag{32}$$

For brevity, we drop the index $m$ from notations for the fluctuation field. The energy then is given by

$$F^{(2)}_{m}[\boldsymbol{\psi}]=\frac{K_1 S}{d}\{S^{(b)}_{m}[\boldsymbol{\psi}]+S^{(s)}_{m}[\boldsymbol{\psi}]\}, \tag{33}$$

$$S^{(b)}_{m}[\boldsymbol{\psi}]=u\int_{-u}^{u}d\tau[[\partial_\tau\boldsymbol{\psi}]^{\dagger}\hat{A}\,\partial_\tau\boldsymbol{\psi}+\tfrac{1}{2}\,\boldsymbol{\psi}^{\dagger}\hat{B}\partial_\tau\boldsymbol{\psi} + \tfrac{1}{2}[\partial_\tau\boldsymbol{\psi}]^{\dagger}\hat{B}^{\dagger}\boldsymbol{\psi}+\boldsymbol{\psi}^{\dagger}\hat{C}\boldsymbol{\psi}], \tag{34}$$

$$S^{(s)}_{m}[\boldsymbol{\psi}]=\sum_{\mu=\pm 1}\boldsymbol{\psi}^{\dagger}\hat{Q}^{(s)}_{\mu}\boldsymbol{\psi}|_{\tau=\mu u}, \tag{35}$$

$$\hat{A}=\begin{pmatrix}r & 0\\ 0 & 1\end{pmatrix},\quad \hat{C}=\begin{pmatrix}1 & 0\\ 0 & r\end{pmatrix}, \tag{36}$$

$$\hat{B}=(r-1)\begin{pmatrix}0 & 1\\ -1 & 0\end{pmatrix}, \tag{37}$$

$$\hat{Q}^{(s)}_{\mu}=\mu u[q_{24}-(1+r)/2]\begin{pmatrix}0 & 1\\ 1 & 0\end{pmatrix}+\begin{pmatrix}w_\phi & 0\\ 0 & w_\theta\end{pmatrix}, \tag{38}$$

where $\partial_\tau\equiv\partial/\partial\tau$ and $S=L_xL_y$ is the area of the substrates. The dimensionless parameters used in Eqs. (34)–(37) are

$$\tau=k_y z,\quad r=\frac{K_2}{K_1},\quad q_{24}=\frac{K_{24}}{K_1}, \tag{39}$$

$$u=\frac{k_y d}{2},\quad w_{\phi,\theta}=\frac{W_{\phi,\theta}d}{2K_1}=\frac{d}{2l_{\phi,\theta}}, \tag{40}$$

where $l_\theta$ and $l_\phi$ are the zenithal and the azimuthal anchoring extrapolation lengths, respectively.

### A. Mirror symmetry and parity of fluctuations

In order to evaluate the correlator of director fluctuations and to study stability of the planar structure, $\mathbf{n}_0=\mathbf{e}_x$, we shall need to solve the Euler-Lagrange equations for the fluctuation energy functional (33):

$$\hat{L}\boldsymbol{\varphi}=0, \tag{41}$$

$$\hat{L}=\hat{A}\partial^2_\tau-\hat{B}\partial_\tau-\hat{C}. \tag{42}$$

These equations are invariant under the mirror symmetry transformation [21]:

$$\boldsymbol{\varphi}(\tau)\rightarrow\hat{P}\boldsymbol{\varphi}(-\tau),\quad \hat{P}=\begin{pmatrix}1 & 0\\ 0 & -1\end{pmatrix}. \tag{43}$$

Algebraically, this result follows because the matrices $\hat{P}$, $\hat{A}$, and $\hat{C}$ are commuting, $\hat{P}\hat{A}-\hat{A}\hat{P}=\hat{P}\hat{C}-\hat{C}\hat{P}=0$, whereas the matrices $\hat{P}$ and $\hat{B}$ anticommute, $\hat{P}\hat{B}+\hat{B}\hat{P}=0$.

The identity $\hat{P}^2=\hat{I}$, where $\hat{I}$ is the identity matrix, shows that invariant sets of the solutions of Eq. (41) can be characterized by the parity with respect to the transformation (43):

$$\boldsymbol{\psi}_{s,a}(-\tau)=\pm\hat{P}\boldsymbol{\psi}_{s,a}(\tau), \tag{44}$$

where $\boldsymbol{\psi}_s$ and $\boldsymbol{\psi}_a$ will be referred to as the symmetric and the antisymmetric fluctuation modes, respectively. For symmetric [antisymmetric] fluctuation fields, the parity relation (44) means that the in-plane and the out-of-plane components $\phi$ and $\theta$ are represented by even [odd] and odd [even] functions of $\tau$, correspondingly: $\phi(-\tau)=\phi(\tau)[\,\phi(-\tau)=-\phi(\tau)]$ and $\theta(-\tau)=-\theta(\tau)[\,\theta(-\tau)=\theta(\tau)]$.

The general solution is now a sum of the symmetric and the antisymmetric modes:

$$\boldsymbol{\varphi}(\tau)=\boldsymbol{\psi}_s(\tau)+\boldsymbol{\psi}_a(\tau). \tag{45}$$

We shall write expressions for the modes in matrix notations through the two fundamental matrices $\hat{\Psi}^{(s)}(\tau)$ and $\hat{\Psi}^{(a)}(\tau)$ composed from solutions of the corresponding symmetry. These $2\times 2$ matrices satisfy both the Euler-Lagrange equation (41) and the parity relation (44). In addition, $\hat{\Psi}^{(\alpha)}(\tau)$ will be conveniently normalized by the condition $\hat{\Psi}^{(\alpha)}(u)=\hat{I}$. It can be verified that solving Eq. (41) yields the following result:

$$\boldsymbol{\psi}_\alpha(\tau)=\hat{\Psi}^{(\alpha)}(\tau)\boldsymbol{\varphi}_\alpha,\quad \alpha=s,a, \tag{46}$$

$$\hat{\Psi}^{(\alpha)}(\tau)=\hat{\Phi}_\alpha(\tau)[\hat{\Phi}_\alpha(u)]^{-1}, \tag{47}$$

$$\hat{\Phi}_\alpha(\tau)=\begin{pmatrix} c_\alpha+\rho\tau s_\alpha & -\rho\tau s_\alpha \\ \rho\tau c_\alpha & s_\alpha-\rho\tau c_\alpha \end{pmatrix}, \tag{48}$$

$$\rho=(1-r)/(1+r), \tag{49}$$

where $c_s=s_a=\cosh\tau$, $s_s=c_a=\sinh\tau$, and $\boldsymbol{\varphi}_\alpha$ are the vectors of integration constants.

After substituting Eqs. (45) and (46) into Eq. (33) and using the symmetry relation (44), we find that the symmetric and the antisymmetric fluctuations independently contribute to the energy of the fluctuation field (45):

$$F_m^{(2)}[\boldsymbol{\varphi}]=\frac{2K_1S}{d}(\boldsymbol{\varphi}_s^\dagger\hat{M}_s\boldsymbol{\varphi}_s+\boldsymbol{\varphi}_a^\dagger\hat{M}_a\boldsymbol{\varphi}_a), \tag{50}$$

$$\hat{M}_\alpha=u(\hat{A}\partial_\tau\hat{\Psi}^{(\alpha)}|_{\tau=u}-\tfrac{1}{2}\hat{B})+\hat{Q}_+^{(s)}. \tag{51}$$

We can now combine Eqs. (36)–(38) and Eqs. (47)–(49) to derive expressions for the matrices $\hat{M}_s$ and $\hat{M}_a$ from Eq. (51). The result is

$$\hat{M}_\alpha=\frac{1}{\beta_\alpha}\begin{pmatrix} m_{11}^{(\alpha)}+w_\phi\beta_\alpha & m_{12}^{(\alpha)} \\ m_{12}^{(\alpha)} & m_{22}^{(\alpha)}+w_\theta\beta_\alpha \end{pmatrix}, \tag{52}$$

$$\beta_{s,a}=\tanh u\mp\rho u(1-\tanh^2 u), \tag{53}$$

where

$$m_{12}^{(\alpha)}=u[q_{24}\beta_\alpha-(1-\rho)\tanh u], \tag{54a}$$

$$m_{22}^{(s)}=m_{11}^{(a)}=(1-\rho)u, \tag{54b}$$

$$m_{11}^{(s)}=m_{22}^{(a)}=m_{22}^{(s)}\tanh^2 u. \tag{54c}$$

### B. Director fluctuations at substrates

Now we apply the analytical results obtained in the preceding section to evaluate the surface part of the correlation function. According to the procedure described in Sec. II B, the first step is to solve the boundary value problem (18) with the Euler-Lagrange equations (41).

It can be readily verified that the fluctuation field $\boldsymbol{\varphi}$ can be written in the form

$$\boldsymbol{\varphi}(\tau)=\hat{\Psi}^{(+)}(\tau)\boldsymbol{\varphi}^{(+)}+\hat{\Psi}^{(-)}(\tau)\boldsymbol{\varphi}^{(-)}, \tag{55}$$

where $\hat{\Psi}^{(+)}=\frac{1}{2}\{\hat{\Psi}^{(s)}+\hat{\Psi}^{(a)}\}$, $\hat{\Psi}^{(-)}=\frac{1}{2}\{\hat{\Psi}^{(s)}-\hat{\Psi}^{(a)}\}\hat{P}$, and $\boldsymbol{\varphi}^{(+)}$ [$\boldsymbol{\varphi}^{(-)}$] is the value of the fluctuation field at the upper [lower] substrate of the cell.

We can now substitute the fluctuation field (55) into the expression for the surface part of the correlator (26) and perform Gaussian integrals with the probability distribution defined in Eqs. (22) and (50) to derive the surface part of the correlator in the final form [27]:

$$\hat{C}^{(s)}(\tau,\tau')=\frac{k_BTd}{2K_1S}\hat{F}(\tau,\tau'), \tag{56}$$

$$\hat{F}(\tau,\tau')=\hat{\Psi}^{(s)}(\tau)\hat{M}_s^{-1}[\hat{\Psi}^{(s)}(\tau')]^\dagger+\hat{\Psi}^{(a)}(\tau)\hat{M}_a^{-1}[\hat{\Psi}^{(a)}(\tau')]^\dagger. \tag{57}$$

This result has also been obtained by means of the Green function method [27].

As is seen from Eq. (57), the surface part of the correlator is a sum of two terms that represent the contributions coming from the symmetric and the antisymmetric fluctuation harmonics at the substrates. The corresponding terms on the right-hand side of Eq. (50) provide expressions for the energies of these harmonics.

We can further emphasize the role of the matrices $\hat{M}_s$ and $\hat{M}_a$. For this purpose, we consider the case in which $\tau=\tau'=\pm u$. Since $\hat{C}^{(b)}(\pm u,\pm u)=0$, the covariance matrix of the director fluctuations at the upper and lower substrates is determined by the correlator (56):

$$\hat{C}^{(s)}(\pm u,\pm u)=\hat{C}(\pm u,\pm u)=\begin{pmatrix} \langle\phi^2\rangle & \langle\theta\phi\rangle \\ \langle\theta\phi\rangle & \langle\theta^2\rangle \end{pmatrix}\Bigg|_{z=\pm d/2}. \tag{58}$$

From Eq. (57) we have

$$\hat{F}(u,u)=\hat{M}_s^{-1}+\hat{M}_a^{-1}, \tag{59}$$

$$\hat{F}(-u,-u)=\hat{P}(\hat{M}_s^{-1}+\hat{M}_a^{-1})\hat{P}. \tag{60}$$

The fluctuations at the substrates are thus entirely described by the matrices $\hat{M}_s$ and $\hat{M}_a$. In Sec. IV D we shall discuss symmetric and antisymmetric fluctuations at the lower substrate of the cell and present some numerical results for the elements of the matrix

$$\hat{P}\hat{M}_\alpha^{-1}\hat{P}=\begin{pmatrix} F_{\phi\phi}^{(\alpha)} & F_{\theta\phi}^{(\alpha)} \\ F_{\theta\phi}^{(\alpha)} & F_{\theta\theta}^{(\alpha)} \end{pmatrix}. \tag{61}$$

From Eqs. (56) and (60) this matrix is proportional to the contribution of the corresponding fluctuation mode to the covariance matrix (58).

## IV. STABILITY OF PLANAR STRUCTURE

In the preceding section we have derived all the analytical results required to perform analysis of the stability conditions (28) efficiently. In our case violating these conditions will render the surface part of the correlator $\hat{C}^{(s)}$ divergent because the energy (50) is not positive definite and the corresponding Gaussian integrals diverge.

Equivalently, the planar structure is stable only if the matrices $\hat{M}_s$ and $\hat{M}_a$ are both positive definite. This yields the following two stability conditions:

$$\det\hat{M}_s>0 \quad \text{and} \quad \det\hat{M}_a>0, \tag{62}$$

which determine stability with respect to the symmetric and the antisymmetric fluctuation modes.

From Eq. (52) explicit expressions for the determinants can be written in the form of a sum of three terms:

$$\det \hat{M}_s = w_\theta w_\phi + \frac{(1-\rho)u}{\beta_s(u)}(w_\theta \tanh^2 u + w_\phi) - u^2 q_{24}\left(q_{24} - 2\frac{(1-\rho)\tanh u}{\beta_s(u)}\right), \tag{63}$$

$$\det \hat{M}_a = w_\theta w_\phi + \frac{(1-\rho)u}{\beta_a(u)}(w_\phi \tanh^2 u + w_\theta) - u^2 q_{24}\left(q_{24} - 2\frac{(1-\rho)\tanh u}{\beta_a(u)}\right), \tag{64}$$

where only the last term can be negative [the functions $\beta_{s,a}(u)$ are defined in Eq. (53) and cannot be negative].

This term is always negative at $q_{24}<0$ and we concentrate on the case of our primary concern in which $q_{24}$ is positive. In this case the term will be negative if the inequality

$$q_{24} > \gamma_\alpha(u) \equiv 2\frac{(1-\rho)\tanh u}{\beta_\alpha(u)} \tag{65}$$

is fulfilled. Given the value of $q_{24}$, the values of the parameter $u$ that satisfy the instability condition (65) form the instability interval for the corresponding fluctuation harmonics.

### A. General method

The key point underlying our analysis is that the determinant $\det \hat{M}_\alpha$ will be negative provided the cell is sufficiently thin and the parameter $u$ lies within the instability interval. The reasoning is as follows.

Given the parameter $u$ $(=k_y d/2)$, which meets the condition (65), the thickness of the cell $d$, which enters Eqs. (63) and (64) through the parameters $w_\theta = d/(2l_\theta)$ and $w_\phi = d/(2l_\phi)$, can be changed independently by varying the fluctuation wave number $k_y$ so as to keep the parameter $u$ fixed. By this means the first two positive terms on the right-hand sides of Eqs. (63) and (64) can be reduced to the limit where the sign of the total sum is determined by the last negative term.

From the above discussion it follows that each value of $u$ from the instability interval defines the critical point where the determinant of the critical mode vanishes. This point is characterized by the thickness of the cell and the fluctuation wavelength, $\lambda = 2\pi/k_y$. The thickness can be computed as a function of $u$ by finding the positive root of the quadratic equation $\det \hat{M}_\alpha = 0$. The wavelength then can be found from the relation $u = k_y d/2 = \pi d/\lambda$ [see Eq. (40)].

Geometrically, these calculations give a set of points $(d,\lambda)$ in the thickness-wavelength plane and by this means the instability interval appears to be mapped onto the curve $\Gamma_\alpha$ in the $d$-$\lambda$ plane. This curve represents the boundary of the instability region for the corresponding fluctuation harmonics.

It is now rather straightforward to carry out the described procedure and derive the parametrization for the curve $\Gamma_\alpha$:

$$\Gamma_\alpha = \begin{cases} D = x_\alpha(u) = u\lambda_\alpha(u)/\pi \\ \Lambda = \lambda_\alpha(u), \end{cases} \tag{66}$$

$$\lambda_s(u) = \frac{\pi}{r_w \beta_s(u)}\{-(1-\rho)(\tanh^2 u + r_w) + [(1-\rho)^2(\tanh^2 u + r_w)^2 + 4r_w \beta_s(u) t_s(u)]^{1/2}\}, \tag{67}$$

$$\lambda_a(u) = \frac{\pi}{r_w \beta_a(u)}\{-(1-\rho)(r_w \tanh^2 u + 1) + [(1-\rho)^2(r_w \tanh^2 u + 1)^2 + 4r_w \beta_a(u) t_a(u)]^{1/2}\}, \tag{68}$$

$$t_\alpha(u) = q_{24}\beta_\alpha(u)[q_{24} - \gamma_\alpha(u)], \tag{69}$$

where the thickness and the wavelength are both conveniently scaled by the zenithal anchoring extrapolation length $l_\theta$:

$$D = \frac{d}{l_\theta}, \quad \Lambda = \frac{\lambda}{l_\theta}, \quad r_w = \frac{W_\phi}{W_\theta}, \tag{70}$$

$D$ is the size parameter; $\Lambda$ is the wavelength parameter; and $r_w$ is the azimuthal anchoring parameter.

Equations (66)–(69) describe the boundary of the instability region provided the instability interval is not empty. So, we discuss the behavior of the functions $\gamma_s(u)$ and $\gamma_a(u)$ that enter the right-hand side of the instability condition (65) and specify the regions of $q_{24}$ in which the instability may occur. The results, illustrated in Fig. 2, are not difficult to obtain analytically.

Figure 2(a) shows that, if the elastic constant $K_2$ is smaller than $K_1$ and $r = K_2/K_1 < 1$, the function $\gamma_a$ increases from $\gamma_a(0) = 2r$ asymptotically approaching the value $\gamma_a(\infty) = 4r/(r+1)$ at large $u$, while $\gamma_s$ is a decreasing function that varies from $\gamma_s(0) = 2$ to $\gamma_s(\infty) = 4r/(r+1)$. As is seen from Fig. 2(b), in the case where $r>1$ the functions $\gamma_a$ and $\gamma_s$ also monotonically approach the common asymptotic value $\gamma_a(\infty) = \gamma_s(\infty) = 4r/(r+1)$. But now we have $\gamma_a(0) = 2r > \gamma_s(0) = 2$.

As we shall see later, there are two qualitatively different regimes of instability depending on whether the instability interval is bounded from above or not. So, we have the two characteristic values of $q_{24}$:

$$q_c^{(1)} = \min(2, 2r), \tag{71}$$

$$q_c^{(2)} = 2(1-\rho) = \frac{4r}{r+1}. \tag{72}$$

Now we pass on to discuss the stability of the planar structure in the intervals separated by these values.

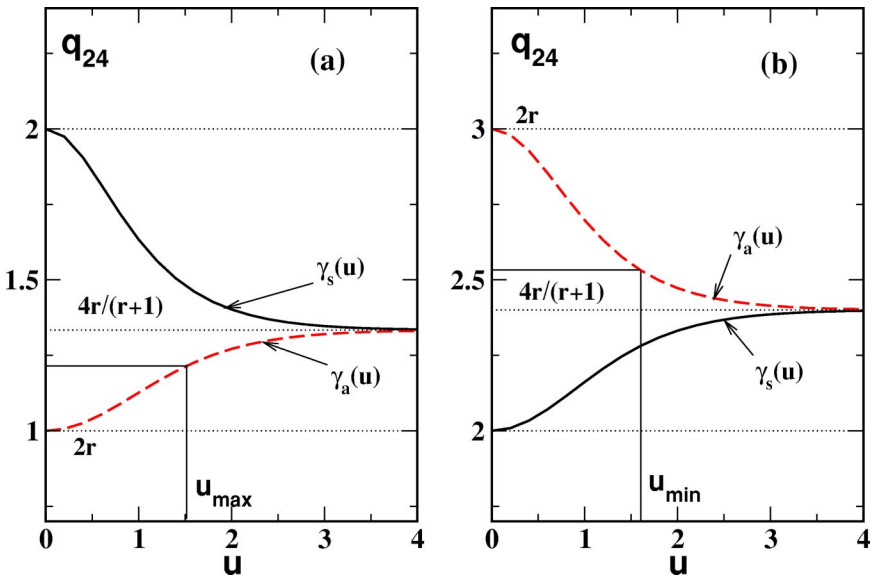


FIG. 2. The graphs of the functions $\gamma_s(u)$ (solid line) and $\gamma_a(u)$ (dashed line) in the $u$-$q_{24}$ plane. Two cases are illustrated: (a) $r<1$ ($r=0.5$) and (b) $r>1$ ($r=1.5$). The end point of the instability interval for the critical mode $u<u_{\max}$ at $q_c^{(1)}<q_{24}<q_c^{(2)}$ is shown on the left. At $q_c^{(2)}<q_{24}<q_c^{(3)}$, the end point of the instability interval for the noncritical mode $u>u_{\min}$ is indicated on the right.

### B. Stability diagrams

In this section we study the stability of the planar structure by analyzing the behavior of the functions which define the boundary curve (66) of the instability region. Qualitatively, the analysis can be performed without resorting to numerical computations and we shall use the numerical results only for illustrative purposes.

Figure 2 clearly indicates the interval

$$0<q_{24}<q_c^{(1)} \tag{73}$$

as the region where the inequalities (65) cannot be satisfied and the structure is stable. The stability conditions (73) are equivalent to the long known Ericksen inequalities (4) derived in Ref. [24]. Figure 3 shows this stability region in the $r$-$q_{24}$ plane.

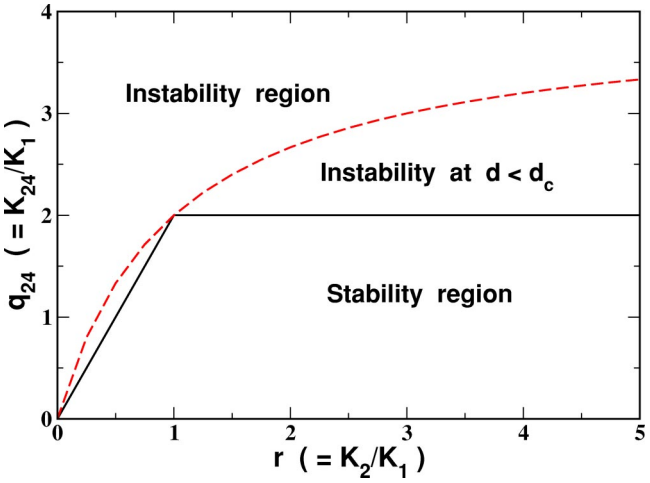


FIG. 3. Stability diagram in the $r$-$q_{24}$ plane. There are two critical values of $q_{24}$ shown as functions of the twist-splay ratio $r$: $q_c^{(1)}$ (solid line) and $q_c^{(2)}$ (dashed line).

Next we consider the interval

$$q_c^{(1)}<q_{24}<q_c^{(2)}, \tag{74}$$

where, as is demonstrated in Fig. 2(a), the instability takes place at $u<u_{\max}$ for the critical fluctuation mode whose symmetry depends on the parameter $r$. For relatively small elastic constants $K_2$ with $r<1$, this mode is antisymmetric [see Fig. 2(a)]. Referring to Fig. 2(b), it can be seen that in the opposite case with $r>1$ the critical mode is symmetric.

Since the instability interval is bounded, the size parameter $D$ on the boundary curve (66) is described by the function $x_\alpha(u)$ and reaches its maximum $D_c$ as $u$ varies from 0 to $u_{\max}$. It follows that in this regime the planar structure is unstable only in sufficiently thin films and $d_c$ ($D_c=d_c/l_\theta$) is the critical thickness. On the curve $\Gamma_\alpha$ this critical point is also characterized by the critical fluctuation wavelength $\lambda_c$ ($\Lambda_c=\lambda_c/l_\theta$).

Since $q_{24}=\gamma_\alpha$ at $u=u_{\max}$, Eqs. (63) and (64) show that the $q_{24}$ dependent term vanishes at $u=0$ and $u=u_{\max}$. When $W_\theta W_\phi\neq 0$, the result is that $x_\alpha(0)=x_\alpha(u_{\max})=0$ and the curve $\Gamma_\alpha$ forms the loop enclosing the region of instability. Figure 4(a) illustrates this result for $r=1.5$ when the boundary curve $\Gamma_s$ is determined by the symmetric critical fluctuation mode.

Thus in this regime the instability induced by the $K_{24}$ term may lead to the formation of periodically modulated structures in cells of subcritical thickness. The critical wavelength $\lambda_c$ provides an estimate for the period of the emerging structure near the critical point.

Now we consider the case of large $q_{24}$ with

$$q_{24}>q_c^{(2)}. \tag{75}$$

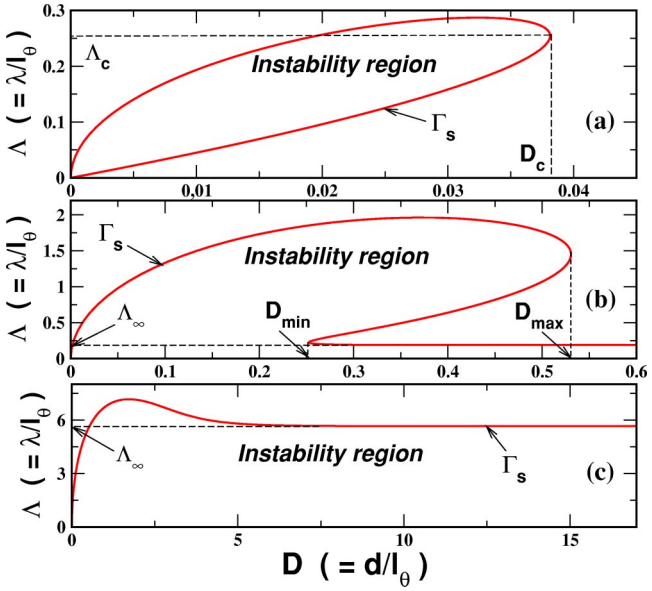


FIG. 4. Stability diagrams in the $D$-$\Lambda$ plane at $W_\phi = W_\theta$ and $r = 1.5$ for various values of $q_{24}$: (a) $q_c^{(1)} = 2 < q_{24} = 2.1 < q_c^{(2)} = 2.4$; (b) $q_c^{(2)} = 2.4 < q_{24} = 2.43 < 2r = 3$; and (c) $2r = 3 < q_{24} = 3.3$.

In this case the instability interval is no longer bounded from above. From Fig. 2 it is clear that the instability condition (65) does not impose any restrictions on $u$ for the critical mode, whereas the instability interval for the noncritical mode is $u > u_{\min}$. Thus, both fluctuation modes lead to the instability at sufficiently large $u$. Equations (67)–(69) provide the limiting value of the functions $\lambda_s(u)$ and $\lambda_a(u)$ at $u \to \infty$:

$$\Lambda_\infty = \frac{\pi}{r_w}\{-(1-\rho)(r_w+1) + [(1-\rho)^2(r_w+1)^2 + 4 r_w q_{24}(q_{24} - q_c^{(2)})]^{1/2}\}, \tag{76}$$

so that the size parameter $D = u\lambda_\alpha/\pi$ increases indefinitely in this limit. The result is that the planar structure is unstable at any thickness of the cell and this instability is caused by the short wavelength fluctuations with $\lambda < \lambda_\infty$. This equally applies to the case of negative $q_{24}$.

Figures 4(b)–4(c) illustrate transformations of the stability diagram in the $D$-$\Lambda$ plane as $q_{24}$ increases beyond $q_c^{(2)}$ at $r > 1$. The curve of the critical mode $\Gamma_s$ forms the boundary of the instability region similarly to the case of the interval (74). The curve of the noncritical mode $\Gamma_a$ resides within this region and is not shown in the figures. Both curves rapidly approach the horizontal asymptote $\Lambda = \Lambda_\infty$.

We show in Fig. 4(b) that, when $q_{24}$ is close to $q_c^{(2)}$, the shape of the curve $\Gamma_s$ still somewhat resembles the loop developed in the interval (74). There are two points marked as $D_{\min}$ and $D_{\max}$ at which the curve bends and at which the function $x_s(u)$ reaches its local minimum and maximum, correspondingly. Further increase of $q_{24}$ reduces the distance between $D_{\min}$ and $D_{\max}$ and the points finally disappear after merging at sufficiently large $q_{24}$. Figure 4(c) presents the stability diagram in this regime.

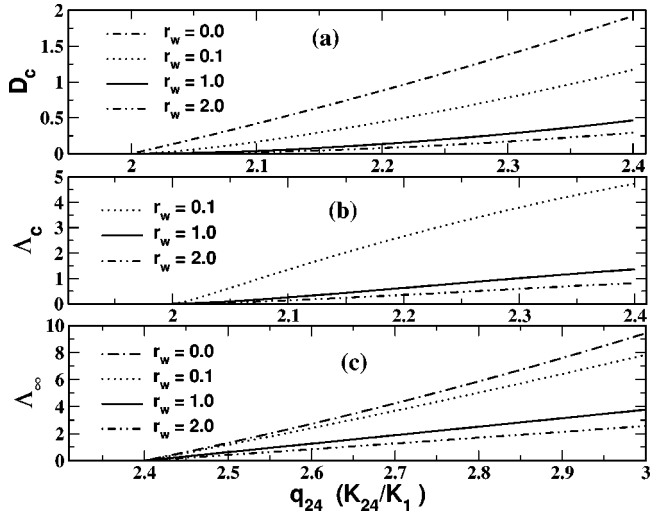


FIG. 5. Dimensionless parameters of (a) critical thickness $D_c$; (b) critical wavelength $\Lambda_c$; and (c) critical asymptotic wavelength $\Lambda_\infty$ $(=\lambda_\infty/l_\theta)$ vs $q_{24}$ at $r = 1.5$ for various values of the azimuthal anchoring parameter $r_w = W_\phi/W_\theta$.

In general, Fig. 3 qualitatively summarizes the results of this section for the three different intervals of $q_{24}$ described in Eqs. (73)–(75). The interval (75) was previously indicated as the instability region in Ref. [21] and as the region where modulated structures can exist in Ref. [25].

### C. Effects of azimuthal anchoring

The critical thickness and the critical wavelength are meaningful only when $q_{24}$ is within the interval (74). By using Eqs. (66)–(69) they both can be computed numerically. The numerical procedure involves two steps: (a) solving the equation $x'_\alpha(u_c) = 0$ to find the maximum of $x_\alpha$ for the critical mode, and (b) evaluating $D_c = x_\alpha(u_c)$ and $\Lambda_c = \lambda_\alpha(u_c)$. The parameter $\Lambda_\infty$ can be computed from Eq. (76).

The critical thickness parameter $D_c$, the critical wavelength parameter $\Lambda_c$, and the parameter $\Lambda_\infty$ as functions of $q_{24}$ for different values of the azimuthal anchoring parameter, $r_w = W_\phi/W_\theta$, are plotted in Figs. 5(a)–5(c). As it can be expected, the curves demonstrate that the structure becomes less stable as the azimuthal anchoring strength decreases. So, in order to estimate the critical thickness from above, it is instructive to discuss the limit of weak azimuthal anchoring, $W_\phi \to 0$, previously considered in Refs. [22,23,25].

In this limiting case the planar structure is marginally unstable with respect to the long wavelength symmetric fluctuations with $k_y = 0$ regardless of $K_{24}$. Mathematically, it follows because the determinant (63) vanishes at $u = 0$ and $w_\phi = 0$. The reason is that all uniform planar structures are energetically equivalent in the absence of azimuthal anchoring.

Nevertheless, we may apply our method to this case by taking the limit $w_\phi \to 0$ in Eqs. (66)–(76) to yield the following result:

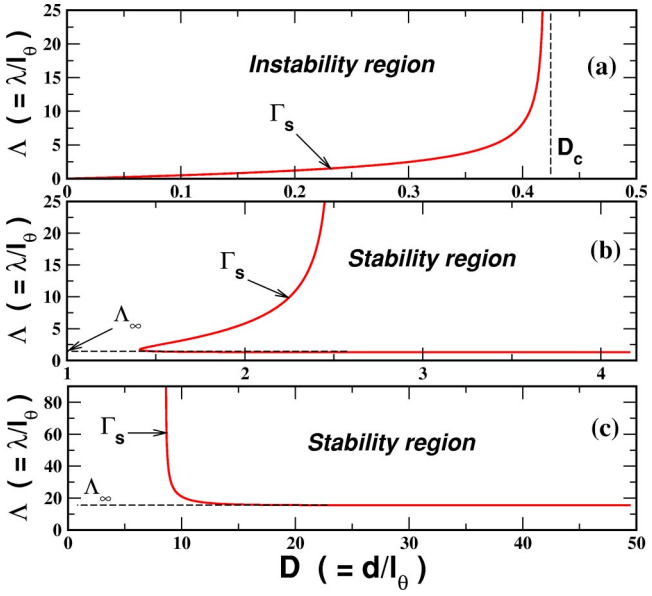


FIG. 6. Stability diagrams in the $D$-$\Lambda$ plane at $r_w=0$ ($W_\phi=0$) and $r=1.5$ for various values of $q_{24}$: (a) $q_c^{(1)}=2<q_{24}=2.1<q_c^{(2)}=2.4$; (b) $q_c^{(2)}=2.4<q_{24}=2.5<2r=3$; and (c) $2r=3<q_{24}=3.3$.

$$\lambda_s(u)=\frac{2\pi t_s(u)}{(1-\rho)\tanh^2 u}, \tag{77}$$

$$\lambda_a(u)=\frac{2\pi t_a(u)}{(1-\rho)}, \tag{78}$$

$$\Lambda_\infty=\lambda_s(\infty)=\frac{2\pi q_{24}}{1-\rho}(q_{24}-q_c^{(2)}). \tag{79}$$

From Eq. (78) it is seen that the behavior of the antisymmetric harmonics at $u=0$ does not differ from the case in which $w_\phi\neq 0$ and $\lambda_a(0)=x_a(0)=0$. But, for the symmetric mode, this is not the case. From Eq. (77) we have $\lambda_s\to\infty$ at $u\to 0$ and

$$D_c=x_s(0)=2q_{24}(q_{24}-2). \tag{80}$$

When $r>1$ and the critical mode is symmetric, Eq. (80) provides the exact expression for the critical thickness at $W_\phi=0$, which has been derived as an approximation in Refs. [22,23,25].

The stability diagrams in the $D$-$\Lambda$ plane at $r>1$ and $W_\phi=0$ are shown in Fig. 6. In the opposite case of $r<1$, so long as $q_{24}<2$ the diagrams are quite similar to those depicted in Fig. 4. Otherwise, at $q_{24}>2$, the noncritical symmetric mode will change the stability diagram presented in Fig. 4(c). The result, however, is not too different from the diagram shown in Fig. 6(c).

If the azimuthal anchoring strength is not identically zero, Eq. (80) estimates the critical thickness from above. In particular, substituting $q_c^{(2)}$ into Eq. (80) and taking the limit $r\to\infty$ we arrive at the conclusion that the critical thickness cannot be larger than $16l_\theta$.

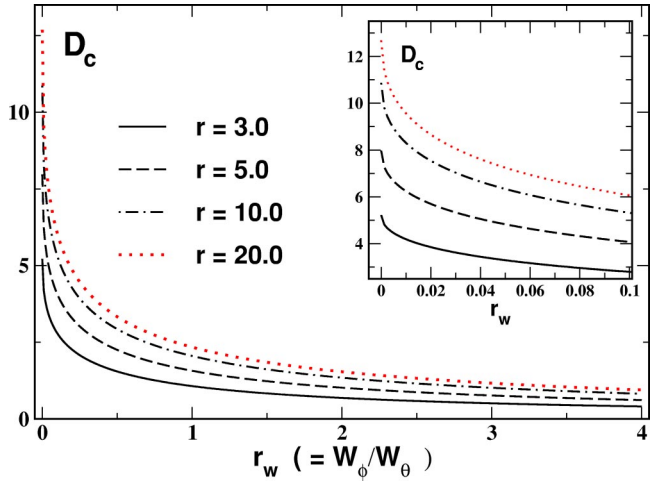


FIG. 7. Dimensionless parameter of critical thickness $D_c$ vs $r_w$ at $q_{24}=q_c^{(2)}-0.1$ for various values of the elastic anisotropy parameter $r$. Inset at the upper right corner enlarges initial decay in the neighborhood of the origin.

Dependencies of the critical thickness $D_c$ and the critical wave number $K_c=2\pi/\Lambda_c$ on the azimuthal anchoring parameter $r_w=W_\phi/W_\theta$ for various values of $r$ are plotted in Figs. 7 and 8. As is seen from Fig. 7, the critical thickness declines steeply in the immediate vicinity of the origin. Typically, the critical thickness at $r_w=0$ appears to be halved at $r_w=0.1$, so that even for $r=20.0$ we need very small azimuthal anchoring $r_w\approx 0.03$ to have $D_c\approx 8$ ($d_c\approx 8l_\theta$). Referring to Fig. 8, the critical wave number $K_c=2\pi/\Lambda_c$ also starts growing rapidly, but the effect is less pronounced at large values of $r$. So, we have $K_c\approx 0.2$ ($k_c\approx 0.2/l_\theta$) at $r_w\approx 0.03$ and $r=20.0$.

When the saddle-splay elastic constant meets a Cauchy relation $K_{24}=(K_1+K_2)/2$ [8,11], we find the two intervals for the twist-splay ratio where the regime of instability defined in Eq. (74) takes place: $3<r<3+2\sqrt{2}\approx 5.82$ and 3

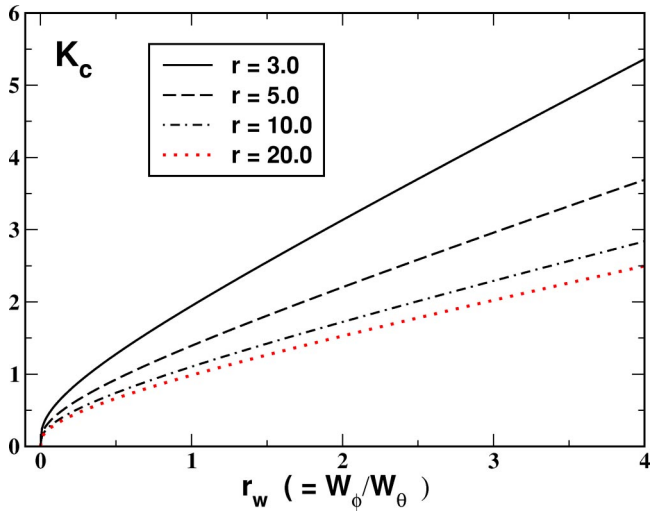


FIG. 8. Dimensionless parameter of critical wave number $K_c$ ($=2\pi/\Lambda_c=k_c l_\theta$) vs $r_w$ at $q_{24}=q_c^{(2)}-0.1$ for various values of the elastic anisotropy parameter $r$.

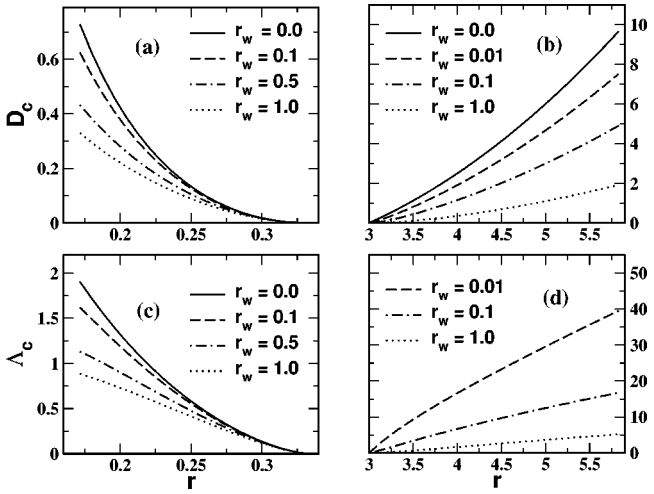


FIG. 9. (a, b) The critical thickness and (c, d) the critical wavelength parameters as a function of the twist-splay ratio $r$ for various values of $r_w$. The graphs are computed by using the Cauchy relation $q_{24}=(1+r)/2$. The saddle-splay parameter $q_{24}$ is in the instability region (74) when $r$ lies in the intervals $3-2\sqrt{2}<r<1/3$ or $3<r<3+2\sqrt{2}$.

$-2\sqrt{2}\approx 0.17<r<1/3$. The critical thickness and the critical wavelength as a function of the parameter $r$ varying within these intervals are plotted in Fig. 9.

For $r<1/3$, the critical fluctuation mode is antisymmetric and Fig. 9(c) shows that the critical wavelength remains finite at $r_w=0$. Referring to Figs. 9(a) and 9(b), the critical thickness at $r<1/3$ is an order of magnitude smaller than in the case where $r>3$ and the critical mode is symmetric.

According to Ref. [23], the latter presents the case in which the ratio $r$ grows anomalously large due to an increase of the twist constant $K_2$ in the vicinity of the nematic-smectic-*A* transition. In this case, the estimate of the critical thickness at $W_\phi=0.0$ and $q_{24}=q_c^{(2)}\approx 3.41$ ($r\approx 5.82$) provides the upper bound for $d_c$ to be about $9.7\,l_\theta$. As is shown in Fig. 9(b), this estimate can be significantly reduced in the presence of azimuthal anchoring.

### D. Director fluctuations at substrates near the critical point

In this section we consider the correlation functions of director fluctuations at the plates bounding the cell by using the results of Sec. III B. Specifically, we shall use Eqs. (58)–(61) that express the correlator in terms of the inverse of the matrices $\hat{M}_s$ and $\hat{M}_a$ given in Eq. (52). We shall restrict our considerations to the stability region where the Gaussian approximation is applicable and study what happens when either the thickness or $q_{24}$ varies so as to get closer to the boundary of the instability region.

In the long wavelength limit $k_y\to 0$ ($u\to 0$), the matrices $\hat{M}_\alpha^{-1}$ are diagonal: $\hat{M}_s^{-1}=\mathrm{diag}(w_\phi^{-1},(w_\theta+1)^{-1})$ and $\hat{M}_a^{-1}=\mathrm{diag}((w_\phi+r)^{-1},w_\theta^{-1})$. It is seen that the correlator diverges at $u=0$ when $W_\phi W_\theta=0$. This is a consequence of the marginal instability discussed in the preceding section.

As far as the large wave number (short wavelength) limit is concerned, it can be shown that in the stability region the matrices (and the correlator) both decay to zero at $u\to\infty$. Interestingly, this is not the case at the boundary of the instability interval when $q_{24}=0$ or $q_{24}=q_c^{(2)}$. In this case we have the nonzero limits $\hat{M}_\alpha^{-1}(\infty)=(w_\theta+w_\phi)^{-1}\left(\begin{smallmatrix}1 & \pm 1\\ \pm 1 & 1\end{smallmatrix}\right)$ for $q_{24}=0$ and $q_{24}=q_c^{(2)}$, respectively. This anomaly is a precursor of the instability caused by short wavelength fluctuations. As a result, using the widespread approximation with $K_{24}=0$ does not give the correlation functions that properly behave at large wave numbers.

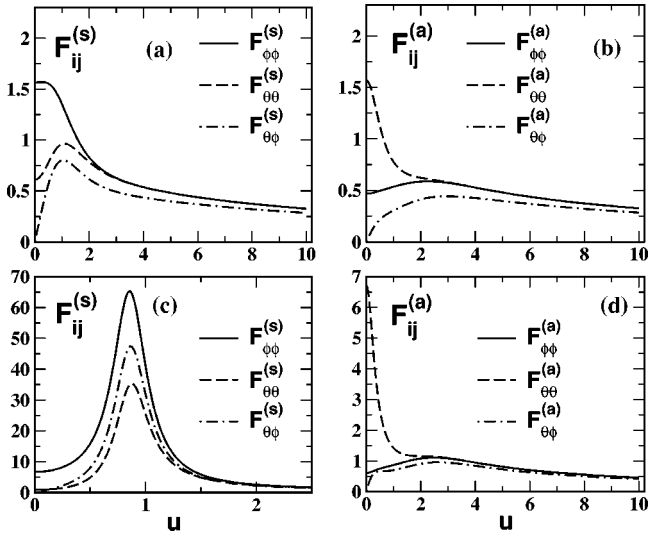


FIG. 10. Elements of the covariance matrix (61) vs $u\times(=k_y d/2)$ for (a) symmetric and (b) antisymmetric fluctuations at the lower substrate, $z=-d/2$, of the cell with the thickness parameter $D=D_c+1.0=1.27$, $q_{24}=q_c^{(1)}+0.3=2.3<q_c^{(2)}$, $r=1.5$, and $r_w=1.0$. The curves shown in (c, d) are computed in the immediate vicinity of the critical thickness at $D=D_c+0.02=0.29$.

We demonstrate in Fig. 10, which shows the spectra of the critical and the noncritical fluctuation modes computed from Eq. (61) at $r=1.5$, that the critical increase of the symmetric fluctuation mode becomes sharply peaked at the critical wave number as the thickness of the cell approaches its critical value. In addition, Fig. 10 shows that the symmetric and the antisymmetric modes are dominated by the in-plane and by the out-of-plane fluctuations, respectively.

## V. DISCUSSION AND CONCLUSIONS

In this paper stability of the uniform director distribution in a planar NLC cell has been studied in the presence of the saddle-splay term. The approach developed to study $K_{24}$ induced instabilities uses the correlation function of the fluctuation field induced by director fluctuations at confining walls (the surface part of the correlator) for derivation of the stability conditions.

This approach in combination with the mirror symmetry considerations has been applied to the case of NLC planar cell. It is found that there are two types of fluctuation modes, which we have called symmetric and antisymmetric modes, depending on the parity under the mirror symmetry transformation involving reflection in the middle plane of the cell.

We have devised the analytical method to analyze the

stability conditions for the fluctuation modes of different symmetry. In this method the thickness of the cell and the fluctuation wavelength form the plane and the boundary of the instability region in this plane is described as a curve defined in the parametric form. The analysis revealed the two different regimes for instabilities caused by the saddle-splay term depending on the value of $K_{24}$.

When $K_{24}$ falls within the range between $2\min(K_1,K_2)$ and $4K_1K_2/(K_1+K_2)$, the planar orientational structure loses its stability only in sufficiently thin cells and the critical thickness $d_c$ together with the wavelength of the critical fluctuation mode, $\lambda_c$, determine the critical point. In this case, as is shown in Fig. 10(c), the spectrum of critical fluctuations at the substrates grows sharply peaked at the critical wavelength when approaching the critical point. The period of modulated structure emerging at the critical point is thus determined by the critical wavelength.

This $K_{24}$ induced instability takes place at any elastic anisotropy parameter $r=K_2/K_1$. The sole exception is the case of elastic isotropy in which $K_1=K_2$. In contrast with the periodic splay-twist Fréedericsz transition [39–41], where spatially modulated pattern comes into play only at sufficiently small twist-splay ratio with $K_2/K_1$, the surface elasticity driven instability cannot be hindered by large elastic anisotropy, but rather, as is shown in Fig. 7, the greater elastic anisotropy the larger the critical thickness can be. The symmetry of the critical fluctuation mode, however, depends on the parameter $r$: the mode is antisymmetric at $r<1$ and is symmetric in the opposite case of $r>1$. Figure 10 shows that the in-plane and out-of-plane fluctuations prevail depending on the symmetry of the fluctuation mode.

The azimuthal anchoring turned out to have a profound effect on both the critical thickness and the critical wavelength. The absence of the azimuthal anchoring presents the limiting case where the planar structure is marginally unstable with respect to the long wavelength fluctuations with $k_y=0$ regardless of the $K_{24}$ term. As a consequence, the critical wavelength $\lambda_c$ increases indefinitely in the limit of weak azimuthal anchoring, $\lambda_c\to\infty$ at $W_\phi\to 0$, while the limiting value of the critical thickness can be computed exactly [see Eq. (80)] giving the upper bound for the critical thickness.

In Sec. IV C, the absolute upper bound for the critical thickness was found to be $16\,l_\theta$. Figure 7 shows that the critical thickness could have been significantly reduced in the presence of relatively small amount of the azimuthal anchoring.

Using the Cauchy relation $K_{24}=(K_1+K_2)/2$ [8,11], we have found that the instability may occur at both sufficiently low and high twist-splay ratios with $r<1/3$ and $r>3$, respectively (see Fig. 9 and the related discussion at the end of Sec. IV C).

The corresponding condition for the periodic Fréedericsz transition requires the ratio $r$ to be below $r_c\approx 0.303$ [40,41] which places a slightly more stringent constraint on the value of $r$ than the above inequality: $r<1/3$. But, as is seen from Fig. 9(a), for small $r$, the critical thickness is an order of magnitude smaller than in the case of large $r$ presented in Fig. 9(b), where $d_c$ can be of order of several microns provided the extrapolation length $l_\theta$ varies in the range $0.1–1\ \mu$m.

For typical nematics, the twist-splay ratio does not exceed unity, but close to the nematic-smectic-*A* transition the parameter $r$ becomes anomalously large [4] leading to the $K_{24}$ induced instability of the ground state at $r>3$. This may result in the appearance of modulated orientational structures as suggested in Ref. [23].

When $K_{24}>4K_1K_2/(K_1+K_2)$ or $K_{24}<0$, the short wavelength fluctuations with $\lambda<\lambda_\infty$ will render the planar structure unstable at any thickness of the cell. With the Cauchy relation such instability will take place when the twist-splay ratio is either less than 0.17 or greater than 5.82. In contrast with the above discussed regime, this instability though does not impose any restrictions on the film thickness, in general, cannot be unambiguously related to the periodic pattern formation. This case requires a more detailed additional study of orientational structures in the instability region where the Gaussian approximation is inapplicable.

Our concluding remark concerns the general method for separating out the contribution of director fluctuations at confining walls to static correlation functions. We have demonstrated that this method can be used as a useful tool for studying orientational instabilities in confined liquid crystals. For this purpose, we have restricted ourselves to the case of uniaxial director fluctuations with uniformly distributed degree of ordering. But a complete treatment of fluctuations at confining surfaces is required in studies of such phenomena as electrohydrodynamical pattern formation [42], instabilities under shear flow [4,43], wetting [44], and backflow [4]. These more general considerations involving fluctuations of spatially varying order parameter tensor coupled to the translational degrees of freedom are well beyond the scope of this paper and we will extend on this subject elsewhere.

## ACKNOWLEDGMENT

The author thanks V. M. Pergamenshchik for useful discussions.

[1] J.W. Doane, in *Liquid Crystals—Application and Uses*, edited by B. Bahadur (World Scientific, Singapore, 1990), Vol. 1, p. 361.

[2] G.P. Crawford and J.W. Doane, Mod. Phys. Lett. B **7**, 1785 (1993).

[3] *Liquid Crystals in Complex Geometries*, edited by G. P. Crawford and S. Žumer (Taylor & Francis, London, 1996).

[4] P.G. de Gennes and J. Prost, *The Physics of Liquid Crystals* (Clarendon Press, Oxford, 1993).

[5] P.M. Chaikin and T.C. Lubensky, *Principles of Condensed Matter Physics* (Cambridge University Press, Cambridge, 1995).

[6] F.C. Frank, Discuss. Faraday Soc. **25**, 19 (1958).
[7] T.C. Lubensky, Phys. Rev. A **2**, 2497 (1970).
[8] J. Nehring and A. Saupe, J. Chem. Phys. **54**, 337 (1971).
[9] S. Faetti, Phys. Rev. E **49**, 4192 (1994).
[10] V.M. Pergamenshchik and S.B. Chernyshuk, Phys. Rev. E **66**, 051712 (2002).
[11] S. Faetti and M. Riccardi, J. Phys. II **5**, 1165 (1995).
[12] H. Yokoyama, Phys. Rev. E **55**, 2938 (1997).
[13] V.M. Pergamenshchik and S. Žumer, Phys. Rev. E **58**, R2531 (1999).
[14] D.W. Allender, G.P. Crawford, and J.W. Doane, Phys. Rev. Lett. **67**, 1442 (1991).
[15] G.P. Crawford, D.W. Allender, and J.W. Doane, Phys. Rev. A **45**, 8693 (1992).
[16] R.D. Polak, G.P. Crawford, B.C. Kostival, J.W. Doane, and S. Žumer, Phys. Rev. E **49**, R978 (1994).
[17] V.M. Pergamenshchik, Phys. Rev. E **47**, 1881 (1993).
[18] A. Sparavigna, O.D. Lavrentovich, and A. Strigazzi, Phys. Rev. E **49**, 1344 (1994).
[19] O.D. Lavrentovich and V.M. Pergamenshchik, Phys. Rev. Lett. **73**, 979 (1994).
[20] O.D. Lavrentovich and V.M. Perganemshchik, Int. J. Mod. Phys. B **12**, 2389 (1995).
[21] A.D. Kiselev and V.Y. Reshetnyak, Mol. Cryst. Liq. Cryst. **321**, 133 (1998).
[22] V.M. Pergamenshchik, Phys. Rev. E **61**, 3936 (2000).
[23] G. Barbero and V.M. Pergamenshchik, Phys. Rev. E **66**, 051706 (2002).
[24] J.L. Ericksen, Phys. Fluids **9**, 1205 (1966).
[25] A.L. Alexe-Ionescu, G. Barbero, and I. Lelidis, Phys. Rev. E **66**, 061706 (2002).
[26] J. Zinn-Justin, *Quantum Field Theory and Critical Phenomena*, 4th ed. (Clarendon Press, Oxford, 2002).
[27] A.D. Kiselev, e-print cond-mat/0309241, http://arXiv.org
[28] H. Kleinert, *Path Integrals in Quantum Mechanics, Statistics and Polymer Physics* (Claredon Press, Oxford, 1999).
[29] A.N. Shalaginov and V.P. Romanov, Phys. Rev. E **48**, 1073 (1993).
[30] A.Y. Val'kov, V.P. Romanov, and A.N. Shalaginov, Sov. Phys. Usp. **164**, 149 (1994).
[31] S. Stallinga, M.M. Wittebrood, D.H. Luijendijk, and T. Rasing, Phys. Rev. E **53**, 6085 (1996).
[32] M.M. Wittebrood, T. Rasing, S. Stallinga, and I. Muševič, Phys. Rev. Lett. **80**, 1232 (1998).
[33] A. Mertelj and M. Copič, Phys. Rev. E **61**, 1622 (2000).
[34] S.A. Pikin, *Structural Transformations in Liquid Crystals* (Gordon and Breach, New York, 1991).
[35] P. Galatola, C. Oldano, and M. Rajteri, Phys. Rev. E **49**, 1458 (1994).
[36] A.D. Kiselev and V.Y. Reshetnyak, JETP **107**, 1552 (1995).
[37] A. Rapini and M. Papoular, J. Phys. (Paris), Colloq. **30**, 54 (1969).
[38] W. Zhao, C.-X. Wu, and M. Iwamoto, Phys. Rev. E **65**, 031709 (2002).
[39] F. Lonberg and R.B. Meyer, Phys. Rev. Lett. **55**, 718 (1985).
[40] W. Zimmermann and L. Kramer, Phys. Rev. Lett. **56**, 2655 (1986).
[41] E. Miraldi, C. Oldano, and A. Strigazzi, Phys. Rev. A **34**, 4348 (1986).
[42] *Pattern Formation in Liquid Crystals*, edited by A. Buka and L. Kramer, (Springer-Verlag, New York, 1996).
[43] A.V. Alonso, A.A. Wheeler, and T.J. Sluckin, Proc. R. Soc. London, Ser. A **459**, 195 (2003).
[44] P. Ziherl, A. Šarlah, and S. Žumer, Phys. Rev. E **58**, 602 (1998).